The Uncertain Future of Massive Binaries Obscures the Origin of LIGO/Virgo Sources

K. Belczynski[1], A. Romagnolo[1], A. Olejak[1] , J. Klencki[2], D. Chattopadhyay[3], S. Stevenson[3] , M. Coleman Miller[4] ,
J.-P. Lasota[1,5] , and Paul A. Crowther[6]

[1] Nicolaus Copernicus Astronomical Center, Polish Academy of Sciences, ul. Bartycka 18, 00-716 Warsaw, Poland; chrisbelczynski@gmail.com,
aleksandra.olejak@wp.pl, amedeoromagnolo@gmail.com
[2] Department of Astrophysics/IMAPP, Radboud University, P.O. Box 9010, 6500 GL Nijmegen, The Netherlands; kklencki@gmail.com
[3] Centre for Astrophysics and Supercomputing, Swinburne University of Technology, John St., Hawthorn, Victoria 3122, Australia; dchattopadhyay@swin.edu.au,
simonpaulstevenson@gmail.com
[4] Department of Astronomy and Joint Space-Science Institute, University of Maryland, College Park, MD 20742-2421, USA; miller@astro.umd.edu
[5] Institut d'Astrophysique de Paris, CNRS et Sorbonne Université, UMR 7095, 98bis Boulevard Arago, F-75014 Paris, France; lasota@iap.fr
[6] Department of Physics & Astronomy, University of Sheffield, Hounsfield Road, Sheffield, S3 7RH, UK; paul.crowther@sheffield.ac.uk

Abstract

The LIGO/Virgo gravitational-wave observatories have detected at least 50 double black hole (BH) coalescences. This sample is large enough to have allowed several recent studies to draw conclusions about the implied branching ratios between isolated binaries versus dense stellar clusters as the origin of double BHs. It has also led to the exciting suggestion that the population is highly likely to contain primordial BHs. Here we demonstrate that such conclusions cannot yet be robust because of the large current uncertainties in several key aspects of binary stellar evolution. These include the development and survival of a common envelope, the mass and angular-momentum loss during binary interactions, mixing in stellar interiors, pair-instability mass loss, and supernova outbursts. Using standard tools such as the rapid population synthesis codes `StarTrack` and `COMPAS` and the detailed stellar evolution code `MESA`, we examine as a case study the possible future evolution of Melnick 34, the most massive known binary star system (with initial component masses of $144\,M_\odot$ and $131\,M_\odot$). We show that, despite its fairly well-known orbital architecture, various assumptions regarding stellar and binary physics predict a wide variety of outcomes: from a close BH–BH binary (which would lead to a potentially detectable coalescence), through a wide BH–BH binary (which might be seen in microlensing observations), or a Thorne–Żytkow object, to a complete disruption of both objects by a pair-instability supernova. Thus, because the future of massive binaries is inherently uncertain, sound predictions about the properties of BH–BH systems formed in the isolated binary evolution scenario are highly challenging at this time. Consequently, it is premature to draw conclusions about the formation channel branching ratios that involve isolated binary evolution for the LIGO/Virgo BH–BH merger population.

Unified Astronomy Thesaurus concepts: Gravitational wave sources (677)

1. Introduction

The LIGO/Virgo Collaboration (LVC) has reported gravitational-wave detections of ∼50 double black hole (BH–BH) coalescences (Abbott et al. 2021). The majority of these can be explained as originating through any of several channels, including isolated binary evolution, dynamics in dense stellar clusters, or primordial BHs (Mandel & Broekgaarden 2021). Until now, observations contained only hints of the possible origin of observed double BHs. For example, as anticipated prior to the detections (Belczynski et al. 2010b), many of the BHs in these binaries have masses ∼$30\,M_\odot$ or larger, which is considerably in excess of the most massive stellar-origin BHs known through electromagnetic observations. Another trend is that the effective spin of the binaries (which is the mass-weighted projection of the BH spins onto the orbital axis) is low; this could be an indication of random orbits from dynamical processes or could point toward intrinsically low spins produced by efficient angular-momentum transport in massive stars (Spruit 2002; Farr et al. 2017; Vitale et al. 2017;

Farr et al. 2018; Qin et al. 2018; Fuller & Ma 2019; Bavera et al. 2020; Belczynski et al. 2020a).

However, there are also individual events with characteristics that may be more challenging to explain and that therefore hold promise for discriminating between formation channels. One such event is GW190814 (Abbott et al. 2020b), which is an extremely asymmetric binary consisting of a ≈$23\,M_\odot$ BH and a $2.6\,M_\odot$ object that is either the lightest BH or the heaviest neutron star (NS) yet detected. Another is the double BH event GW190521 (Abbott et al. 2020a), which has two BHs that may have masses of ∼$85\,M_\odot$ and ∼$65\,M_\odot$, putting them both in the pair-instability mass gap, although it is possible that the BH mass ratio is farther from unity and both BHs avoid the gap (Fishbach & Holz 2020; Nitz & Capano 2021).

Based on these results, several groups have recently analyzed the BH–BH population as a whole, with special attention to outliers such as GW190814 and GW190521, to obtain insight into the relative fraction of events from different formation channels. For example, Zevin et al. (2021) studied a mixture of isolated binary evolution and dynamical formation in globular clusters and concluded that neither channel can contribute more than 70% to the LIGO/Virgo observed population of BH–BH mergers. In contrast, Ossowski (2021) disfavored the globular cluster channel in favor of isolated

binary evolution. Franciolini et al. (2021) investigated four formation channels (isolated binaries, globular clusters, nuclear star clusters, and primordial BHs) and found a high likelihood that primordial BH–BH mergers are part of the LIGO/Virgo source population.

All of these studies perform proper model comparison to infer which model or mixture of models is favored. However, model comparison requires precisely specified models, i.e., models with precisely defined physics. Here we emphasize that the physics uncertainties (Schootemeijer et al. 2019) in at least one of those models, of isolated binary evolution, are sufficiently large that (to put it in Bayesian terms) the prior dominates the conclusion. That is, different assumptions can lead to very different outcomes, which means that population studies that employ models of isolated binary evolution are not yet at a stage allowing strong and credible conclusions to be drawn, even if other models were uncertainty free.

We demonstrate these model weaknesses using various, different assumptions in performing simulations whose aim is to determine the fate of the most massive known binary system. Despite the high binary frequency of massive stars (Sana et al. 2012), eclipsing systems with primary masses $\gg 50 \, M_\odot$ are exceptionally rare. Within the Milky Way, the most extreme double-lined systems are located in young, rich star clusters: A1 within NGC 3603 (Schnurr et al. 2008), F2 within the Arches (Lohr et al. 2018), and WR20a in Westerlund 2 (Bonanos et al. 2004). All three are short-period (days), low-eccentricity systems with main-sequence Wolf-Rayet (H-rich, WNh) primaries.

The most massive double-lined eclipsing system in the Large Magellanic Cloud (LMC) is also a short-period system, Hunter 38 in the Tarantula Nebula with an O-type primary, whose mass is $\sim 57 \, M_\odot$ (Massey et al. 2002). The most extreme LMC binaries are noneclipsing systems, also within the Tarantula Nebula. They have minimum dynamical primary masses in excess of $\sim 50 \, M_\odot$, albeit with orbits whose periods are an order of magnitude longer and with high eccentricities. From comparison with Bonn stellar evolutionary models at LMC metallicity (Brott et al. 2011), R139 ($P_{orb} = 154$ d, $e = 0.38$) has a primary O supergiant mass of $\sim 80 \, M_\odot$ (Mahy et al. 2020), R144 ($P_{orb} = 74$ d, $e = 0.51$) has a primary WNh mass of $\sim 110 \, M_\odot$ (Shenar et al. 2021), and Melnick 34 (Mk 34, $P_{orb} = 155$ d, $e = 0.68$)—the current record holder—has component WNh+WNh masses of $139^{+21}_{-18} \, M_\odot$ and $127 \pm 17 \, M_\odot$ (Tehrani et al. 2019) with initial masses of $144 \, M_\odot$ and $131 \, M_\odot$. Pollock et al. (2018) first established that Mk 34 is a colliding wind binary from an analysis of X-ray time-series observations, while Tehrani et al. (2019) noted that the potential fate of Mk 34 involves a double stellar-mass BH binary merger.

We predict the fate of Mk 34, using different physics assumptions, by applying two rapid population synthesis codes (StarTrack and COMPAS) and the detailed stellar evolutionary code (MESA). We find a wide variety of possible outcomes (see Table 1) in terms of the BH masses and orbital separations, and even in terms of whether BHs will form at all. We therefore urge caution in drawing important and credible conclusions about the LVC BH–BH population based on models of massive-binary evolution containing, by necessity, uncertain physics.

Table 1
Fate of Mk 34

Model	M_{BH1} ($M_\odot$)	M_{BH2} ($M_\odot$)	t_{delay} (Myr)	Fate
StarTrack1	22.5	22.1	47.5	close BH–BH?[a]
StarTrack2	35.7	33.3	10,035	close BH–BH?[a]
StarTrack3	36.0	32.5	11,663	close BH–BH?[a]
COMPAS1	19.8	20.2	$>t_{hub}$	wide BH–BH
COMPAS2	31.8	31.7	$>t_{hub}$	wide BH–BH
COMPAS3	31.8	31.7	$>t_{hub}$	wide BH–BH
MESA1	21.9	51.6[b]	⋯	Thorne–Żytkow
MESA2	35.2	80.9[b]	⋯	Thorne–Żytkow
MESA3	35.3	85.4[b]	⋯	Thorne–Żytkow
Pavlovskii1	21.9	22.1	$>t_{hub}$	wide BH–BH
Pavlovskii2	35.2	33.3	$>t_{hub}$	wide BH–BH
Pavlovskii3	⋯	⋯	3.3	stellar merger[c]
QuasiSingle1	⋯	⋯	⋯	PSN+PSN[d]
QuasiSingle2	~ 60	$\sim 60 \, M_\odot$	$>t_{hub}$	wide BH–BH
QuasiSingle3	~ 30	$\sim 30 \, M_\odot$	$>t_{hub}$	wide BH–BH
QuasiSingle4	~ 20	$\sim 20 \, M_\odot$	$>t_{hub}$	wide BH–BH

Notes.
[a] Optimistic (nonstandard) StarTrack models are used to get this result.
[b] For MESA models we list the CE donor mass in column M_{BH2}.
[c] Merger of post-MS star and MS star: formation of a very massive single star, fate: PSN or a single BH.
[d] Pair-instability supernovae disrupting binary components.

2. Calculations

For the initial properties of Mk 34, we select $M_a = 144 \, M_\odot$, $M_b = 131 \, M_\odot$, $e = 0.68$, and $a = 760 \, R_\odot$, chosen to result in an orbital period of $P_{orb} = 155$ days after 0.6 Myr (current age; Tehrani et al. 2019) of system evolution with the StarTrack code. We adopt the LMC metallicity of $Z = 0.006$ (Rolleston et al. 2002).

2.1. StarTrack Calculations

We use the population synthesis code StarTrack (Belczynski et al. 2020a), which employs analytic fits to evolutionary tracks of nonrotating stellar models (Hurley et al. 2000). We adopt standard wind losses for massive stars from Vink et al. (2001) and luminous blue variable (LBV) winds as $(dM/dt)_{lbv} = f_{lbv} 10^{-4} \, M_\odot \mathrm{yr}^{-1}$ with $f_{lbv} = 1.5$ from Belczynski et al. (2010a).

For stars that overfill their Roche lobes, we initiate mass transfer between binary components and associated (if any) mass loss from binary systems. If the binary is not circularized by tidal interactions, we circularize it ($e_{new} = 0$) to periastron distance ($a_{new} = a(1 - e)$) in one time step and only then start Roche lobe overflow (RLOF). For nuclear-timescale mass transfer (NTMT) and thermal-timescale mass transfer (TTMT), we use the standard formalism, while we use a diagnostic mass ratio diagram as a criterion for common-envelope (CE) development (see Section 5 of Belczynski et al. 2008). During the TTMT/NTMT, the fraction of mass lost by the donor star that is accumulated by nondegenerate companion stars is set to $f_a = 0.5$, while the rest is lost with specific angular momentum (expressed in units of $2\pi a^2/P_{orb}$) of $j_{loss} = 1.0$ (see Equation (33) of Belczynski et al. 2008). The accumulation of mass on

compact objects (e.g., NS/BH) is limited by the (Eddington) critical accretion rate and mass is lost with the specific angular momentum of the compact accretor (King et al. 2001; Mondal et al. 2020).

We employ the delayed core-collapse supernova (SN) engine in the NS/BH mass calculation (Fryer et al. 2012), which allows for the lower mass gap between NSs and BHs to be populated (Belczynski et al. 2012; Zevin et al. 2020). We employ a weak pair-instability pulsation supernova (PPSN) mass-loss and pair-instability supernova (PSN) model that results in the upper mass gap: no BHs with mass $M_{BH} \gtrsim 55\,M_\odot$ (Belczynski et al. 2020a). We allow for the fallback-decreased NS/BH natal kicks with $\sigma = 265$ km s^{-1} and no natal kicks for direct BH formation. This is our standard input physics marked as "StarTrack1" model in Table 1.

The development of the CE phase is a big issue in stellar/binary astrophysics (Ivanova et al. 2013b; Olejak et al. 2021). We are agnostic about which systems should be sent to a CE and which should evolve through stable RLOF. In Star-Track models we allow for the most optimistic scenario (see Section 3.1), and we send nearly all systems through the CE to form (potentially) BH–BH mergers. We do not do this on regular basis. According to our standard input physics, donors with radiative envelopes (e.g., in the Hertzsprung gap) do not enter the CE phase. Because it is not fully understood how exactly a CE develops, we test various assumptions to show how these influence the future fate of binary systems such as Mk 34. Contrasting models are being presented as well.

During CE events the entire envelope of the donor is assumed to be lost from the binary, with the exception of compact object companions that are allowed to accrete a small fraction of the donor's envelope at 5% of the Bondi rate (MacLeod et al. 2017a). The CE orbital decay is calculated with the standard energy-balance formalism (Webbink 1984) in which we adopt 100% efficiency of the orbital energy transfer ($\alpha = 1.0$) into the envelope, while the binding energy is parameterized by detailed stellar models (λ scaling: Xu & Li 2010; Dominik et al. 2012).

In "StarTrack2" we decrease wind mass-loss rates for LBV stars to $f_{lbv} = 0.48$ and we increase the He-core mass at the end of the main sequence by a factor of $f_{core} = 1.5$ with respect to the original Hurley et al. (2000) models. This model approximately reproduces the basic properties of the $131\,M_\odot$ and $144\,M_\odot$ models at the terminal-age main-sequence (TAMS) obtained in our MESA computations (see Section 2.3).

In "StarTrack3" we circularize massive binaries with angular-momentum conservation ($a_{new} = a(1 - e^2)$), we set $j_{loss} = 0.1$, and $f_a = 0.25$ while keeping the rest of the input physics as in "StarTrack2." This model aims to test the survival of the CE phase in an Mk 34-like future evolution (see Section 3). In practice, such a setup allows the secondary star of Mk 34 to have a large radius (wide binary orbit) during the RLOF and therefore potentially to develop a convective envelope but to survive the CE phase.

2.2. COMPAS Calculations

We use the population synthesis code COMPAS (Stevenson et al. 2017; Vigna-Gómez et al. 2018; Chattopadhyay et al. 2021), which incorporates stellar (Hurley et al. 2000) and binary evolution (Hurley et al. 2002) with updated wind prescriptions for massive stars (Vink et al. 2001; Belczynski

et al. 2010a). The LBV wind losses are as in StarTrack (see Section 2.1).

In its default setup, the mass accretion during RLOF onto degenerate stars (i.e., BHs, NSs, and white dwarfs) is Eddington limited in COMPAS. For nondegenerate stars, this accretion limit is set by the ratio of the rate at which mass is being donated to the rate at which mass can be incorporated into the companion star. These two rates, in turn, are determined by the thermal (Kelvin–Helmholtz) timescales of the donor and the companion, respectively (Kalogera & Webbink 1996). The thermal timescale is an explicit function of the mass, radius, and luminosity of the star. For a star of total mass M, envelope mass M_{env}, radius R, and luminosity L, the thermal timescale τ_{KH} is given by $\tau_{KH} = GMM_{env}/RL$, where G is the universal gravitational constant. In binaries, because these stellar parameters are determined by the orbital period at which the donor overflows its Roche lobe, the thermal timescale of the donor becomes an implicit function of the orbital properties of the binary (Schneider et al. 2015). Thus, the accretion efficiency in binaries is primarily determined by their orbital period. The mass transfer efficiency β_{acc} (ratio of the mass gained by the donor to the mass lost from the companion)[7] in a nondegenerate star can be thus expressed as $\beta_{acc} = \min(1, 10^{\frac{\tau_{KH,acc}}{\tau_{KH,don}}})$, where $\tau_{KH,acc}$ and $\tau_{KH,don}$ are the thermal timescales of the accretor and donor, respectively (Hurley et al. 2002; Schneider et al. 2015; Chattopadhyay et al. 2021).

The stability of the mass loss is determined by the parameter ζ (critical mass–radius exponent for development of CE) in COMPAS using fits from the Ge et al. (2015) simulations as described in Vigna-Gómez et al. (2018). In nearly equal-mass, close binaries, the thermal timescales of the donor and accretor being very similar, the mass transfer is usually conservative and remains stable. In close systems with a more extreme mass ratio, the thermal timescale of the donor being much longer than the accretor, the mass transfer becomes nonconservative leading to a CE phase. The Ge et al. (2015) criteria render the mass transfer from evolved (non-main-sequence, nondegenerate) massive stars as predominantly stable (Neijssel et al. 2019), which is very similar to the Pavlovskii et al. (2017) model (discussed in Section 2.4). We assume an isotropic reemission model for angular-momentum loss during nonconservative stable RLOF (Pols et al. 1998).

Unlike in StarTrack, the binary is not circularized right before RLOF (Vigna-Gómez et al. 2018). But binaries that survive the CE events are always circularized (Vigna-Gómez et al. 2018). All other default RLOF and CE mass-transfer specifications in COMPAS are identical to StarTrack as described in Section 2.1.

Our standard model COMPAS1 utilizes the Fryer et al. (2012) "delayed" supernovae prescription and presupernova core mass to postsupernova remnant mass mapping. The (pulsational) PSN modeling is implemented in COMPAS (Stevenson et al. 2019) with polynomial fitting from the models by Marchant et al. (2019) as the default input. The natal kick distributions (including fallback) for BHs and NSs are identical to the StarTack1 model.

In the model COMPAS2 we reduce the LBV wind mass-loss rate to $f_{lbv} = 0.48$ (from $f_{lbv} = 1.5$ in COMPAS1). We also increase the He-core mass of the terminal-main-sequence stars

---

[7] Equivalent of the parameter f_a in StarTrack described in Section 2.1.

Table 2
Dutch Stellar Winds in MESA[a]

	$T_{eff} < 10^4$ K	$T_{eff} \geqslant 10^4$ K
...	de Jager et al. (1988)	...
$H_{sur} < 0.4$	...	Nugis & Lamers (2000)
$H_{sur} \geqslant 0.4$	...	Vink et al. (2001)

Note.
[a] Based on T_{eff}, winds either depend or do not depend on H_{sur}.

by a factor of $f_{core} = 1.5$ multiplied to the fitting formula from Hurley et al. (2000) (Equation (30)). COMPAS2, like StarTrack2, is adjusted to approximately reproduce the total mass and the core mass at TAMS of the $131\,M_\odot$ and $144\,M_\odot$ models computed with MESA.

The model COMPAS3 is identical to COMPAS2 but here we allow the binary to circularize (while conserving its angular momentum) right before the onset of RLOF as detailed for StarTrack in Section 2.1.

2.3. MESA Calculations

2.3.1. Calibration of TAMS Core Masses

The fitting formula by Hurley et al. (2000) to the evolutionary tracks from Pols et al. (1998), which are the basis for the StarTrack and COMPAS population synthesis codes, are based on stellar models computed for stars with masses up to $40\,M_\odot$. The treatment of more massive stars in StarTrack and COMPAS relies on extrapolation. In the mass range considered in this study (130–145 $M_\odot$), this can lead to a significant deviation in basic stellar properties from what detailed stellar models produce (or what is inferred from observations). One property that is particularly inaccurate due to the extrapolation of the Hurley et al. (2000) formulae (and which is crucial for considerations of the final fate of the Mk 34 system) is the ratio of the helium core mass to the total star mass at TAMS ($M_{core,TAMS}/M_{TAMS}$). For very massive stars this ratio is close to unity (Yusof et al. 2013; Köhler et al. 2015). In contrast, a $144\,M_\odot$ star at $Z = 0.006$ metallicity evolved with StarTrack or COMPAS, even though significantly stripped through MS winds ($M_{TAMS} = 77.4\,M_\odot$), is far away from being a helium star with the helium core mass of only $M_{core,TAMS} = 34.1\ M_\odot$.

To correct for this and calibrate the properties of the StarTrack and COMPAS models at TAMS, we use the MESA 1D stellar evolution code (Paxton et al. 2011, 2013, 2015, 2018, 2019).[8] We compute single models of $131\,M_\odot$ and $144\,M_\odot$ stars at $Z = 0.006$ metallicity. The relative initial abundances of metals follow Grevesse et al. (1996). We model convection by using mixing-length theory (Böhm-Vitense 1958) with a mixing-length parameter $\alpha = 2.0$, and we adopt the Schwarzschild criterion for convection. We used the Dutch wind setup in MESA, which combines different prescriptions depending on the effective temperature T_{eff} and the fractional surface hydrogen abundance H_{sur}. As shown in Table 2, for $T_{eff} < 10^4$ K, the code uses the mass-loss rates from de Jager et al. (1988), regardless of the hydrogen surface abundance. For $T_{eff} \geqslant 10^4$ K, MESA adopts either the Nugis & Lamers (2000) prescriptions (if $H_{sur} < 0.4$) or mass-loss rates

---

[8] MESA version r15140, http://mesa.sourceforge.net/.

Table 3
Properties of MESA Models Used to Calibrate the Population Synthesis Simulations (the Two Top Rows) as well as a Few Models with Increased Wind Mass Loss or Core Overshooting (See Section 2.3.2)

Model	R_{Max} ($R_\odot$)	M_{TAMS} ($M_\odot$)	$M_{core,TAMS}$ ($M_\odot$)
144 $M_\odot$ ($\delta_{ov} = 0.12$, $f_{wind} = 1$)	>1968	94	67
131 $M_\odot$ ($\delta_{ov} = 0.12$, $f_{wind} = 1$)	>2000	87	58
144 $M_\odot$ ($\delta_{ov} = 0.33$, $f_{wind} = 1$)	46	62	61
131 $M_\odot$ ($\delta_{ov} = 0.33$, $f_{wind} = 1$)	41	59	58
144 $M_\odot$ ($\delta_{ov} = 0.12$, $f_{wind} = 1.5$)	40	57	55
131 $M_\odot$ ($\delta_{ov} = 0.12$, $f_{wind} = 1.5$)	40	63	53

Note. We show the maximum radius reached in our simulation as well as the total mass and the He-core mass at the end of the MS phase.

from Vink et al. (2001) (if $H_{sur} \geqslant 0.4$). Additionally, mass-loss rates in MESA can be increased or decreased by changing a specific scaling factor f_{wind}. The standard prescription of Vink et al. (2001) is known to underestimate the empirical mass-loss rates of very massive MS stars, which increase dramatically as they approach the Eddington limit, Γ_e (Vink et al. 2011; Bestenlehner et al. 2014; Bestenlehner 2020). Indeed, clumping-corrected mass-loss rates of the components of Mk 34 from Tehrani et al. (2019) exceed the Vink et al. (2001) prescriptions by factors of 2–3.

We account for convective overshooting above the hydrogen-burning core by applying the step overshooting formalism, which extends the convective core by a fraction δ_{ov} of the local pressure scale height.

We initialize our models with the initial rotation of $V_i = 250\ \mathrm{km\,s^{-1}}$ (guided by the analysis of Tehrani et al. 2019). For rotational mixing, we include the effects of the Eddington–Sweet circulation, secular shear instabilities, and the Goldreich–Schubert–Fricke instability, with an efficiency factor $f_c = 1/30$ (Heger et al. 2000; Brott et al. 2011).

We avoid using the MLT++ option in MESA (Paxton et al. 2013). As a result, models that reach the red supergiant stage encounter numerical difficulties in their superadiabatic outer envelope layers (Pavlovskii & Ivanova 2015; Klencki et al. 2020), which prohibit us from following their evolution to the point of maximum radial expansion. However, for the purpose of the current study, we are only interested in the properties of MESA models at TAMS as well as whether or not the models expand sufficiently to lead to an RLOF in the Mk 34 binary system. We thus stop the MESA computations when the radius of $2000\,R_\odot$ is reached. Otherwise, we stop the simulation after 10,000 MESA steps. Such stopping conditions are sufficient for our purposes in all the considered scenarios for the Mk 34 system.

For the calibration of population synthesis models at TAMS, we calculate a MESA stellar model with initial mass $M_{ZAMS} = 144\,M_\odot$, metallicity $Z = 0.006$, and $V_i = 250\ \mathrm{km\,s^{-1}}$. We apply the standard Dutch winds ($f_{wind} = 1.0$, though see above) and step overshooting of $\delta_{ov} = 0.12$ to maintain consistency with the overshooting in models by Pols et al. (1998) and the Hurley et al. (2000) fits. At the end of the MS, this model has a mass of $M_{TAMS} = 94.0\,M_\odot$ with a He-core mass of $M_{core,TAMS} = 66.6\ M_\odot$ (see Table 3). Post-MS expansion leads to a maximum radius of $R_{max} = 1968\ R_\odot$ at the end of our simulation, at which point the star is still expanding as a red supergiant. A MESA stellar

model with $M_{\mathrm{ZAMS}} = 131\,M_\odot$, $Z = 0.006$, and $V_\mathrm{i} = 250\,\mathrm{km\,s^{-1}}$ results in $M_{\mathrm{MS}} = 86.6\,M_\odot$ and $M_{\mathrm{core}} = 58.5\;M_\odot$ and expands beyond $2000\,R_\odot$ (see Table 3).

The $M_{\mathrm{ZAMS}} = 144\,M_\odot$ ($Z = 0.006$) nonrotating Star-Track or COMPAS model produces $M_{\mathrm{TAMS}} = 77.4\,M_\odot$ and $M_{\mathrm{core,TAMS}} = 34.1\;M_\odot$. We decrease the winds during MS, keeping the original Vink et al. (2001) prescriptions, but decreasing the LBV winds to $f_{\mathrm{lbv}} = 0.48$ to get a model with $M_{\mathrm{TAMS}} = 94.2\,M_\odot$ and $M_{\mathrm{core,TAMS}} = 44.5\;M_\odot$. Next, we increase the core size by $f_{\mathrm{core}} = 1.5$ to get the target values: $M_{\mathrm{TAMS}} = 94.2\,M_\odot$ and $M_{\mathrm{core,TAMS}} = 66.7\;M_\odot$ in the population-synthesis codes. Note that such a massive star is already luminous ($L \sim 3 \times 10^6\,L_\odot$) and cold enough ($T_{\mathrm{eff}} \sim 30,000$ K) to be beyond the Humphreys–Davidson limit (Humphreys & Davidson 1994) and subject to LBV winds on the MS. Applying the same calibration to $M_{\mathrm{zams}} = 131\,M_\odot$ ($Z = 0.006$) we obtain in population synthesis codes: $M_{\mathrm{MS}} = 89.5\,M_\odot$ and $M_{\mathrm{core}} = 62.3\;M_\odot$. We apply this calibration for all metallicities. However, one should note that some observations may be in contradiction of metallicity-independent LBV winds (Gilkis et al. 2021).

2.3.2. Calibration of Post-MS Expansion

When considering the future fate of the Mk 34 system, a key question is whether its very massive components will expand after the end of the MS and initiate a mass-transfer interaction or whether they will lose their hydrogen envelopes already during the MS and smoothly transition to become compact helium stars, avoiding any RLOF. The two crucial aspects that affect the degree of the post-MS expansion of very massive stars are the amount of core overshooting and the strength of stellar winds. Here, we explore this by computing a small grid of MESA models with different overshooting and wind assumptions.

For the calibration of the TAMS properties of the $131\,M_\odot$ and $144\,M_\odot$ models, we assumed a modest core overshooting of $\delta_{\mathrm{ov}} = 0.12$, following the calibration to low-mass stars in open clusters by Pols et al. (1998). More recently, Choi et al. (2016) found the best agreement with the properties of the Sun for a MESA model with $\delta_{\mathrm{ov}} = 0.16$. However, there is an increasing amount of evidence that core overshooting could be significantly larger in the case of massive stars (e.g., Brott et al. 2011; Castro et al. 2014; Claret & Torres 2018; Scott et al. 2021). In particular, the calibration by Brott et al. (2011) to match the observed drop in rotational velocities of post-MS B stars (although see Vink et al. 2010) resulted in $\delta_{\mathrm{ov}} = 0.33$, a value that has become widely used to compute stellar models of massive stars in the recent years. On the other hand, there is no observational calibration of core overshooting in the case of very massive stars of masses above $100\,M_\odot$. As such, we explore six different δ_{ov} values from a wide range between 0.12 and 0.5.

The Dutch wind scheme in MESA incorporates the Vink et al. (2001) prescription for optically thin line-driven winds of hot MS stars. However, as noted above, very massive stars possess a sufficiently high luminosity to mass ratio on their MS that they approach their Eddington limit, leading to high mass-loss rates (Gräfener & Hamann 2008; Vink et al. 2011; Bestenlehner et al. 2014; Bestenlehner 2020). Here, we attempt to correct for this by simply increasing the wind scaling factor f_{wind} from 1.0 to 1.5 or to 2.0.

We compute a grid of $131\,M_\odot$ and $144\,M_\odot$ models with the above variations in overshooting and winds (and all the other assumptions same as in our calibration models in Section 2.3.1). All of the results are shown in Appendix and a few selected examples in Table 3. In short, we find that any model with overshooting of $\delta_{\mathrm{ov}} = 0.33$ or higher, or a wind multiplication factor $f_{\mathrm{wind}} \geqslant 1.5$ evolves to become a helium Wolf-Rayet star already by the end of MS, avoiding radial expansion beyond $100\,R_\odot$ and any RLOF interaction in the Mk 34 binary. This result is at the basis of the quasi-single evolutionary scenario for Mk 34; see Section 2.5.

2.3.3. Calibration of Envelope-binding Energies

Recent studies by Klencki et al. (2021) and Marchant et al. (2021) have shown that the envelope-binding energies used in StarTrack and COMPAS (i.e., λ scaling following Xu & Li 2010; Dominik et al. 2012) may be severely underestimated in the case of massive stars with outer radiative envelopes. Note that population synthesis codes do not perform CE evolution for Hertzsprung-gap stars (radiative outer envelope) under standard assumptions on input physics, but typically the CE is applied for core-helium-burning stars even for those with outer radiative envelopes.

To explore the effect of revised binding energies on the future fate of Mk 34, whenever our StarTrack binary evolution calculation predicts a CE phase to occur, we use MESA to compute a detailed stellar model of the donor star. We then follow the method outlined in Klencki et al. (2021) to integrate through the envelope of the MESA model and compute its binding energy. When matching the properties of a MESA model with those from StarTrack, we ensure that the CE donor has the same helium core mass and the same radius but allow for a lower envelope mass in the MESA model, so that we may be under- but never overestimating the envelope-binding energy. This allows for conservative statements on the inability of a binary to eject the donor's envelope and the CE survival.

2.4. Pavlovskii Calculations

Models presented below are obtained with the modified StarTrack. In particular, we use more restrictive criteria for the CE development (Pavlovskii et al. 2017) and allow more binaries to evolve through stable mass transfer instead (Olejak et al. 2021). The new criteria are applied (i) to H-rich post-MS donor stars, (ii) for initial masses larger than $18\,M_\odot$, (iii) when the mass ratio (companion to donor mass at CE onset) fulfills the condition $q_{\mathrm{CE}} < q_{\mathrm{crit}}$ for the CE to develop, where $q_{\mathrm{crit}} = 0.19$–0.36 depending on donor mass and metallicity, and (iv) when the donor's radius at the onset of CE fulfills specific criteria (shown in Figures 2 and 3 of Olejak et al. 2021) for the CE to develop. These new criteria lead to the emergence of BH–BH formation channels without CE in StarTrack simulations (Olejak et al. 2021). This is the same channel that was proposed by van den Heuvel et al. (2017) and that is also found in several other simulations (Neijssel et al. 2019; Stevenson et al. 2019; Shao & Li 2021).

Models labeled "Pavlovskii1" and "Pavlovskii2" correspond to models "StarTrack1" and "StarTrack2" but with modified CE development criteria, respectively.

In model "Pavlovskii3" we test different formulae for the loss of the angular momentum during mass transfer through the L2 point given by MacLeod & Loeb (2020):
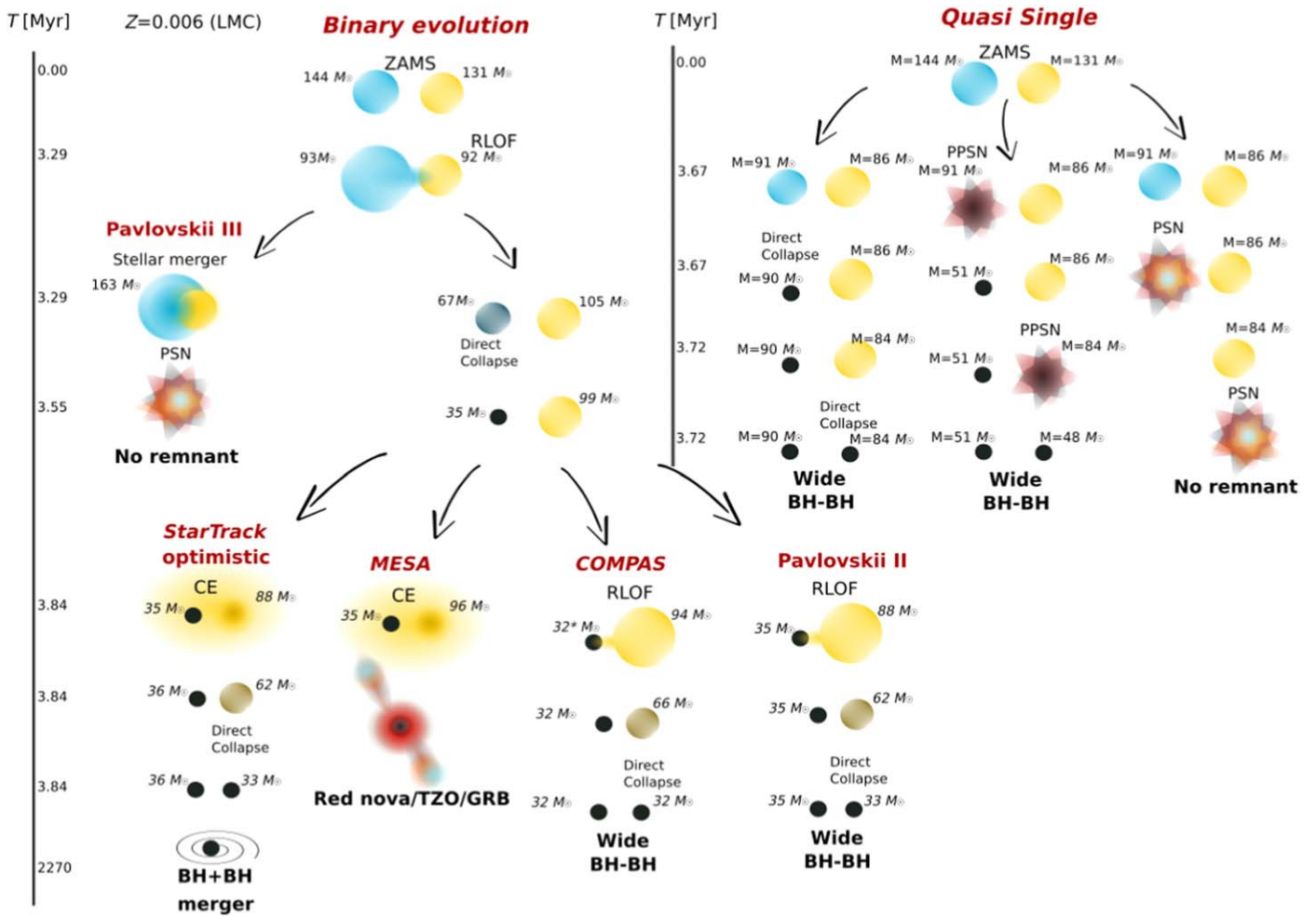
Figure 1. Future evolution of Melnick 34. The fate of this massive binary is subject to a number of stellar and binary evolution uncertainties. Depending on the adopted evolutionary model, Mk 34 may form a close or wide BH–BH system, a Thorne–Żytkow (TZ—Thorne & Żytkow 1977) object, or end its life in two PSNe. RLOF: Roche lobe overflow, CE: common envelope, TTMT: thermal-timescale mass transfer, ZAMS: zero-age main sequence, BH: black hole, GRB: gamma-ray burst, PPSN: pair-instability pulsation supernova. *: COMPAS track gives a somewhat lower-mass BH (formed out of an initially more massive star) than other binary scenarios.

$j_{\rm loss} = j_{\rm L2} = 1.2^2 \frac{M_{\rm tot}^2}{M_{\rm don} M_{\rm acc}}$ instead of our standard $j_{\rm loss} = 1.0$ (Podsiadlowski et al. 1992). We expect a much higher loss of angular momentum with this modification, which may result in another potential fate for the future evolution of Mk 34 (see Section 3.4). The rest of the input physics of "Pavlovskii3" corresponds to "Pavlovskii2." A change of the circularization scheme would only increase binary orbital separation.

2.5. Quasi-single-star Calculations

In this part we approximate the evolution of nonexpanding components of Mk 34. Radial expansion of massive stars can be quenched due to extensive mass loss in stellar winds (e.g., Conti 1975; Vanbeveren 1991; Vanbeveren et al. 1998; Langer 2012; Smith 2014). For stars above $\gtrsim 40\,M_\odot$, this may be the reason behind the observational scarcity of red supergiants above the empirical Humphreys–Davidson limit (Humphreys & Davidson 1979, 1994). The more massive a star, the stronger the mass loss in winds. As a result, stars as massive as the components of Mk 34 may become helium-rich Wolf-Rayet stars already during the MS and avoid any significant post-MS expansion.

We find this behavior for MESA models with sufficiently large overshooting or increased stellar winds (see Table A). In particular, MESA models with $\delta_{\rm ov} = 0.33$ and standard winds ($f_{\rm wind} = 1.0$) reach a maximum radius of $46\,R_\odot$ for $M_{\rm ZAMS} = 144\,M_\odot$ and $41\,R_\odot$ for $M_{\rm ZAMS} = 131\,M_\odot$. Additionally, important for the development of the PPSN/PSN, stellar models that do not expand may have very different TAMS helium core masses. For example, the $M_{\rm ZAMS} = 144\,M_\odot$ model produces $M_{\rm core,TAMS} = 61\ M_\odot$ for $\delta_{\rm ov} = 0.33$ and $f_{\rm wind} = 1.0$ or $M_{\rm core,TAMS} = 30\ M_\odot$ for $\delta_{\rm ov} = 0.4$ and $f_{\rm wind} = 1.5$. The former model is possibly subject to a PPSN/PSN while the latter is not (Woosley 2017; Farmer et al. 2020).

In Section 3.5 we explain our choice of models, showing how uncertainties can affect the future evolution of Mk 34.

3. Examples of Mk 34's Future Evolution

Various predicted models of Mk 34's future evolution are illustrated in Figure 1, summarized in Table 1, and described below.

3.1. StarTrack Models

A binary star resembling Mk 34 is evolved with the StarTrack2 model (Section 2.1). Star A (initially more massive) expands as it evolves and finally periodically overfills its Roche lobe ($R_a = 139\,R_\odot$) at periastron passages. At this point, the orbit expanded from the initial $a = 760\,R_\odot$ to $1125\,R_\odot$ due to wind mass loss from both binary components ($M_a = 94.2\,M_\odot$, $M_b = 91.9\,M_\odot$) while the eccentricity remained much unchanged ($e = 0.68$). The tidal circularization force is the strongest at periastron, and we assume that the orbital motion is circularized to periastron distance and leads to normal stable RLOF on a new ($a = 360\,R_\odot$) circular orbit. RLOF leads first to TTMT, which subsequently transforms to an NTMT. Star A is stripped almost entirely of its H-rich envelope ($M_a = 67.4\,M_\odot$, $M_{a,core} = 67.3\,M_\odot$) while star B accreted half of that lost envelope ($M_b = 105\,M_\odot$) while the rest of the mass has been lost from the binary. In response, the orbit increased in size ($a = 439\,R_\odot$). Star A is a Wolf-Rayet with heavy wind mass loss and at the end of its nuclear evolution its mass decreases to $M_a = 35.6\,M_\odot$ ($a = 1370\,R_\odot$, $M_b = 99.1\,M_\odot$). Star A collapses directly to a BH with a mass of $M_a = 35.2\,M_\odot$ (1% neutrino mass loss, no baryonic mass loss, no natal kick). Then star B evolves and expands to fill its Roche lobe in a circular orbit with $a = 1515\,R_\odot$ ($M_b = 88.5\,M_\odot$, $R_b = 700\,R_\odot$, $T_{b,eff} = 8690$ K). This time in our standard approach, due to the relatively high mass ratio ($q = 88.5/35.2 = 2.5$), RLOF is evaluated to lead to a CE phase. We estimate the binding energy of star A's envelope ($\lambda = 0.103$) to be low enough to be ejected at the cost of orbital energy. After envelope ejection, star B becomes a massive stripped He core ($M_b = 62.0\,M_\odot$) and the orbit decays to $a = 34.2\,R_\odot$. During CE the first-formed BH accretes $\sim 0.5\,M_\odot$ ($M_a = 35.7\,M_\odot$). Star B, after a Wolf-Rayet wind mass loss ($M_b = 33.7\,M_\odot$, $a = 47.8\,R_\odot$), collapses directly to a BH ($M_b = 33.3\,M_\odot$). After $t_{evol} = 4.1$ Myr of binary evolution, a close BH–BH binary is formed with a coalescence time of $t_{coal} = 10.0$ Gyr.

There are caveats in this scenario. Star B at the time of the RLOF onset has just finished core H fusion and is a Hertzsprung-gap star in the transition to become a core-He burning giant. It was argued that such stars do not have a clear core-envelope structure and that the CE phase should always lead to the merging of the donor star with its companion (Belczynski et al. 2007). This finds some support in observations as the predicted BH–BH merger rates that allow for such a scenario as presented above are too high to match the empirical LIGO/Virgo estimate (see submodels A in Table 4 of Belczynski et al. 2020a). In addition, star B has an outer radiative envelope: at the time of RLOF and with surface properties $R_b = 700\,R_\odot$, $T_{b,eff} = 8690$K $\rightarrow L = 2.5 \times 10^6\,L_\odot$, it is well above the effective temperature threshold below which stars at LMC metallicity have convective envelopes ($T < 3900$ K; see Figure 6 of Klencki et al. 2020). Klencki et al. (2021) argued that massive radiative-envelope giants have binding energies that are too high to allow for a successful CE ejection in BH–BH merger progenitor binaries. In StarTrack models, the estimate of the binding energy of star B with the λ formalism is only an approximation that is needed for use in rapid population synthesis models. It should be also stressed that in the standard input physics of StarTrack models we would allow no Hertzsprung-gap star to survive a CE phase no matter our estimate of the star binding energy (λ) or assumed efficiency of orbital energy transfer to the envelope (α). This is

why we call the StarTrack models used here optimistic scenarios. We test this optimistic estimate with MESA in Section 3.3.

In the StarTrack1 model a similar scenario develops. However, because the stars and their cores are less massive, the BH masses are $\sim 10\,M_\odot$ smaller than in model StarTrack2 (see Table 1).

In the StarTrack3 model we adjust evolutionary parameters in such a way that CE survival is less caveated than in model StarTrack2. We alter the circularization process, and we change the RLOF parameters, setting mass transfer/loss to obtain a wider binary than in the StarTrack2 model. This allows star B to expand more before it initiates the CE phase: $R_b = 1439\,R_\odot$, $a = 3141\,R_\odot$, $M_b = 85.9\,M_\odot$, $M_{b,core} = 60.1\,M_\odot$, $T_{b,eff} = 5986$ K, $\lambda = 0.050$. This star almost has a convective envelope, but not quite so. If we perform CE energy balance with the above parameters this system survives CE and forms close BH has BH binary at $t_{evol} = 3.9$ Myr and with $t_{coal} = 11.7$ Gyr. Yet, the same caveats remain as for the StarTrack2 model.

3.2. COMPAS Models

With the initial masses, orbital period, and eccentricity of Mk 34 (see Section 2) we evolve the COMPAS1, COMPAS2, and COMPAS3 models with the individual variations specified in Section 2.2. As in Section 3.1, we will always refer to the originally more massive star (with $M_{ZAMS} = 144\,M_\odot$) as star A.

In the COMPAS2 model, star A ends core-H burning with a total mass of $94.2\,M_\odot$, while the stellar winds increase the separation to $a = 1165.3\,R_\odot$. As star A leaves the MS, its core mass is calculated to be $M_{a,core} = 66.8\,M_\odot$. Star A overfills its Roche lobe soon during post-MS evolution losing its envelope ($27.4\,M_\odot$) in a stable (fully conservative) TTMT RLOF phase. This is the outcome of the binary being fairly wide and the donor being an evolved (post-MS) star, as commented on in Section 2.2 (see also Schneider et al. 2015). Eccentricity remains unchanged ($e = 0.68$) during this phase and the orbit expands to $a = 1374.9\,R_\odot$. Star B, which had a total mass of $91.8\,M_\odot$ right before the mass transfer, becomes a $119.2\,M_\odot$ MS star. Being stripped off its H-rich envelope, star A enters the naked helium-star (Wolf-Rayet) phase with mass $M_a = 66.8\,M_\odot$. Evolution continues while both stars are losing mass in winds. Star A with mass $M_a = 35.4\,M_\odot$ undergoes direct core collapse, forming a BH of mass $M_a = 31.8\,M_\odot$, while star B with $M_b = 115.3\,M_\odot$ is still on the MS. The orbital separation, right after the formation of BH A, becomes $a = 1712.1\,R_\odot$. Star B leaves the MS with mass $M_b = 93.7\,M_\odot$ and core mass $M_{b,core} = 66.3\,M_\odot$ when the orbital separation is $a = 2006.6\,R_\odot$. Shortly thereafter star B fills its Roche lobe, loses most of its H-rich envelope ($\sim 27.3\,M_\odot$), and becomes a naked helium star in stable TTMT RLOF. The post-RLOF orbital separation is decreased to $a = 918.1\,R_\odot$. Eddington limited accretion allows BH A to gain only $\sim 3.7 \times 10^{-5}\,M_\odot$. The binary at the onset of this RLOF, though has a slightly smaller separation than the previous RLOF phase, is still fairly wide and results in a stable TTMT RLOF despite a rather high mass ratio ($q = 93.7/31.8 = 2.9$). It is noted that both RLOF phases noted in the COMPAS2 model are fairly similar to the Pavlovskii2 model (see Section 3.4). However, the binary remains eccentric through both RLOF phases ($e = 0.673$). Star B, with a mass $M_b = 35.2\,M_\odot$, undergoes direct core-collapse and forms a BH of $31.7\,M_\odot$. COMPAS2 model creates a BH–BH system, which at the

second BH formation has a separation $a = 1372.6 R_\odot$ and an eccentricity of $e = 0.658$. This wide BH–BH system does not merge in a Hubble time.

The evolution within the COMPAS1 model is fairly analogous to the COMPAS2 model. However, higher wind mass loss and less internal mixing lead to the formation of a much less massive BH–BH system. BHs in this model are $\sim 20 M_\odot$ while in COMPAS2 they are $\sim 32 M_\odot$. The orbital separation at BH–BH formation is $a = 740.6 R_\odot$ while the eccentricity remains virtually unchanged ($e = 0.68$), resulting in a coalescence time longer than the Hubble time.

Results of evolution in the COMPAS3 model are also broadly similar to those of the COMPAS2 model (see Table 1). The additional condition of pre-RLOF orbital circularization, however, changes a few key points. The first RLOF (stable, TTMT, star A to star B) decreases the orbital separation from $11,165.6 R_\odot$ to $739.2 R_\odot$ and the eccentricity becomes $e = 0.0$. As star B evolves, stellar winds increase this orbital separation to $a = 1097.3 R_\odot$ right before the second RLOF (stable, TTMT, star B to BH A). At this point, the eccentricity is $e = 0.023$, increased from the previous circularization at the formation of the first BH. The second RLOF decreases the separation to $a = 501.9 R_\odot$, and again the orbit is circularized. The binary orbital separation at the time of formation of the BH–BH system (with $\sim 32 M_\odot$ BHs) becomes $a = 779.6 R_\odot$ while the orbital eccentricity is negligible ($e = 0.054$). Though the COMPAS3 model evolution decreases the binary orbital separation substantially, we note that this change is not significant enough to create a close double BH system that merges in a Hubble time.

We note that COMPAS3 creates the closest BH–BH binary obtained in the three COMPAS models. We note that to create a similarly circularized double BH system with the same masses, which merges within a Hubble time, the orbital separation at BH–BH formation can at most be about $46.7 R_\odot$ (Peters 1964). A highly eccentric orbit can also decrease the merger time. However, for a BH–BH system with the same masses and orbital separation as in the COMPAS3 model, this cutoff eccentricity should be at least $e = 0.98$.

Interestingly, the structure of the BH X-ray binary Cyg X-1 (though a less massive system than Mk42) was used in StarTrack (Wiktorowicz et al. 2014) and COMPAS (Neijssel et al. 2021) calculations to argue that the future evolution of Cyg X-1 (Miller-Jones et al. 2021) may also lead to a wide BH–BH system, which will not merge in a Hubble time.

3.3. MESA Models

In this section we use the MESA code to check the outcome of the CE phase encountered in the three StarTrack models from Section 3.1 (see Section 2.3.3 and Klencki et al. 2021, for the method).

In the model MESA2 we evolve a star with $M_{\rm zams} = 133 M_\odot$, overshooting $\sigma_{\rm ov} = 0.2$ and Dutch winds with $f_{\rm wind} = 1.5$. This model produces at some point of its post-MS evolution a star with a mass of $M = 80.9 M_\odot$ and a He-core mass of $M_{\rm core} = 62.2 M_\odot$, radius of $R = 700 R_\odot$, and $T_{\rm eff} \approx 9000$K (an outer radiative envelope; the envelope would not become convective until least $T_{\rm eff} \lesssim 4500$K Klencki et al. 2020). At this point we calculate the envelope-binding energy (obtained from integration of the mass distribution over the entire envelope) corrected for the internal energy of the envelope, then we subtract the BH accretion luminosity that effectively lowers

binding energy, to obtain $E_{\rm bind} = 6.67 \times 10^{50}$ erg. This translates to $\lambda_{\rm MESA} = 0.012$. This model resembles star B at the onset of CE in the StarTrack2 example of evolution. The orbital energy at the onset of CE is $E_{\rm orb,i} = -0.04 \times 10^{50}$ erg and the post-CE separation is $a = 6.2 R_\odot$ (corresponding to a post-CE $E_{\rm orb,f} = -6.81 \times 10^{50}$ erg). This was obtained under the assumption of a 100% efficiency of the orbital energy transfer to unbind the envelope ($\alpha = 1.0$). The radius of the exposed core of star B is $2.84 R_\odot$ (Hurley et al. 2000 formulae) while its new Roche lobe is only $2.64 R_\odot$, and we assume a CE merger in such case. In the StarTrack2 model, the binding energy ($\lambda = 0.103$) was underestimated as it scales with $\propto 1/\lambda$ by a factor of ~ 9 as compared with detailed MESA estimate ($\lambda = 0.012$).

Note that because the BH accretes part of the envelope during the CE inspiral (for the numerical treatment of this process, see the Appendix in Belczynski et al. 2002), the binary does not need to balance the entire binding energy of the envelope ($E_{\rm bind}$) with the orbital energy ($E_{\rm orb,f} - E_{\rm orb,i}$). However, this has no influence on our conclusion above. Accretion onto the BH is estimated at the level of $\sim 0.5 M_\odot$ (see Section 2.1), while this MESA model underestimates the mass of the stellar envelope found in StarTrack2 simulation by $\sim 7.4 M_\odot$ ($M_{\rm env} = 26.1 M_\odot$ in StarTrack2 simulation, and $M_{\rm env} = 18.7 M_\odot$ in the above MESA simulation).

The other two population synthesis models from StarTrack also produce CE mergers (Thorne–Żytkow objects) if the MESA binding energy estimate is used. In the StarTrack1 model the CE donor was estimated to have $\lambda = 0.050$, while the MESA calculation gives $\lambda = 0.007$. In the StarTrack3 model, $\lambda = 0.050$ in contrast with the MESA estimate of $\lambda = 0.008$.

In all the cases considered above, the CE donor was a massive radiative-envelope star. The prediction that the CE phase in BH binaries with such donors most likely leads to mergers was recently voiced by Klencki et al. (2021) and Marchant et al. (2021). If so, this would leave the remaining case of massive convective-envelope donors (i.e., red supergiants) as the only possible CE channel for the formation of BH–BH mergers, as first suggested by Mennekens & Vanbeveren (2014). Based on the observational scarcity of red supergiants above $\sim 40 M_\odot$, these authors concluded that the contribution of CE evolution in the formation of massive BH–BH mergers could in fact be close to zero.

3.4. Pavlovskii Models

A binary star resembling Mk 34 is evolved with the Pavlovskii2 model (Section 2.4). Evolution to RLOF initiated by star B is the same as in the StarTrack2 model ($\lesssim 1\%$ differences in binary parameters are numerical). However, here the binary undergoes stable RLOF: TTMT instead of CE. During mass exchange/mass loss the orbital separation changes from $a = 1507 \rightarrow 928 R_\odot$ and star B is stripped from its H-rich envelope ($M_{\rm b} = 87.7 \rightarrow 62.3 M_\odot$), becoming a massive Wolf-Rayet star. Accretion onto the BH is negligible as the mass transfer was highly supper-Eddington ($M_{\rm a} = 35.2 \rightarrow 35.2 M_\odot$) and the loss of angular momentum (given the mass ratio at the onset of RLOF: $q = 87.7/35.2 = 2.5$) causes the orbit to decrease in size by a factor of 1.6; this may be compared with the orbital decrease by a factor of 63 during CE in the StarTrack2 model. After Wolf-Rayet wind mass loss ($M_{\rm b} = 33.9 M_\odot$, $a = 1427 R_\odot$) star B collapses

directly to a BH ($M_b = 33.3 \, M_\odot$). After $t_{evol} = 4.16$ Myr of binary evolution, a wide BH–BH binary is formed with a coalescence time of $t_{coal} = 6.0 \times 10^6$ Gyr.

In the Pavlovskii1 model, the binary follows a similar evolution, but a lower-mass wide BH–BH binary forms ($21.9 + 22.1 \, M_\odot$) due to the stronger winds and lower core masses adopted in this model (see Table 1).

In the Pavlovskii3 model, due to the strongly increased loss of the orbital angular momentum during TTMT, the system does not survive the first TTMT. It ends with a stellar merger of the Hertzsprung-gap-star donor ($M_a = 80.2 \, M_\odot$) with its main-sequence star companion ($M_b = 98.9 \, M_\odot$). The actual mass and the fate of the stellar-merger product are uncertain. Both observations and simulations of stellar mergers are usually related to low-mass stars, which are not BH progenitors (Lombardi et al. 2002; Tylenda & Kamiński 2016) or are calculated for dynamical collisions in dense stellar clusters (Glebbeek et al. 2013). It seems that a rather low mass fraction is lost during stellar mergers (Lombardi et al. 2002, 2006; Glebbeek et al. 2013). Assuming that the merger product in our simulation will become a Hertzsprung-gap star with the mass of $\sim 163 \, M_\odot$ (similarly to the scheme used in Olejak et al. (2020) with 20% of the less massive star being ejected during the merger) the single star will end its evolution either (i) as PSN leaving no remnant if classical PSN models are used (Woosley 2017; Leung et al. 2019) or (ii) as a single $\sim 30–40 \, M_\odot$ BH, if nonstandard PSN models are used (see Figure 1 of Belczynski 2020 and references therein).

The amount of angular-momentum loss through the L2 Lagrangian point adopted in the Pavlovskii3 model, $j_{loss} = j_{L2} = 1.2^2 \frac{M_{tot}^2}{M_{don} M_{acc}} \in [5.76, 5.82]$,[9] is considered to be an upper limit whereas the standard StarTrack $j_{loss} = 1.0$ used in models Pavlovskii1 and Pavlovskii2 is instead close to the lower limit as indicated by MacLeod et al. (2018) and MacLeod & Loeb (2020). The maximal possible j_{loss}, which allows a stellar merger to be avoided during the first TTMT and would lead to the formation of a wide BH–BH binary from Mk 34, is $j_{loss} \in [3.74, 3.92]$ (65% of j_{L2} of MacLeod & Loeb 2020). This demonstrates that even with increased angular-momentum losses, it is possible to form either a wide BH–BH binary ($t_{delay} > t_{hub}$) with a minimal separation of about $a = 609 \, R_\odot$ ($t_{delay} = 2.6 \times 10^5$ Gyr $> t_{hub}$) or a stellar merger but not a close BH–BH system.

3.5. Quasi-single-star Evolution Models

Based on MESA models (see Appendix), current literature, and simple estimates, we follow the future evolution of the Mk 34 binary with nonexpanding stars. We put the two stars on an eccentric ($e = 0.68$) and wide orbit ($a = 780 \, R_\odot$). These stars lose $\gtrsim 100 \, M_\odot$ during their MS life in stellar winds, expanding the orbital separation ($a > 1000 R_\odot$; see Section Appendix). At the post-MS closest encounter of these two stars (periastron), the Roche lobe radii of both components are $R_{lobe} > 100 \, R_\odot$. The radii of both stars are $R < 100 \, R_\odot$ for many MESA models. There is no mass exchange between the stars.

Depending on (i) the mass and core mass of nonexpanding stellar models and (ii) the mass (in reality central temperature and density) and the range allowed for the onset of a PPSN/

PSN, we can envision several different outcomes of Mk 34's future evolution.

If both stars have core masses as high as $61 \, M_\odot$ and $58 \, M_\odot$ at TAMS (see MESA models with $\delta_{ov} = 0.33$ and $f_{wind} = 1.0$ in Appendix), these cores will reach $65 \, M_\odot$ at the time of oxygen burning, which will then become explosive leading to PSN (Woosley 2017). Each star gets disrupted, leaving no compact object remnant but producing a luminous PSN (model: QuasiSingle1; see Table 1).

There is a significant caveat to the above prediction. According to recent studies (Woosley 2017; Limongi & Chieffi 2018; Farmer et al. 2020; Costa et al. 2021; Farrell et al. 2021), very low-metallicity stars can produce BHs with mass as high as $\sim 80–90 \, M_\odot$. But there are also detailed MESA stellar evolutionary models that allow for the formation of BHs with $\sim 70 \, M_\odot$, avoiding a PPSN/PSN (Belczynski et al. 2020b) at high metallicity. If this scenario is adopted, then it is expected that a $60 + 60 \, M_\odot$ wide BH–BH binary would form ((model: QuasiSingle2).

For lower-mass stars/cores at TAMS, we expect to avoid a PPSN/PSN and we predict the formation of a wide BH–BH binary. For example, if we take MESA models with $\delta_{ov} = 0.4$ and $f_{wind} = 1.5$ they will produce stars with $M = 32 \, M_\odot$ ($M_{core,TAMS} = 30 \, M_\odot$) and $M = 32 \, M_\odot$ ($M_{core,TAMS} = 30 \, M_\odot$). These stars are not subject to PPSN/PSN and depending on the post-MS stellar wind mass loss will form $\sim 30 \, M_\odot$ BHs (model: QuasiSingle3). The formation of a wide BH–BH binary, with coalescence time exceeding the Hubble time, is predicted.

If we push MESA models even further to higher overshooting and stronger winds ($\delta_{ov} = 0.5$ and $f_{wind} = 2.0$), we produce stars with $M = 21 \, M_\odot$ ($M_{core,TAMS} = 19 \, M_\odot$) and $M = 21 \, M_\odot$ ($M_{core,TAMS} = 19 \, M_\odot$) at TAMS. This will also lead to the formation of a wide BH–BH binary but with $\sim 20 \, M_\odot$ BHs at most (model: QuasiSingle4).

4. Discussion

We have investigated the future evolutionary tracks and fate of the most massive known binary system, Mk 34. Several interesting possibilities seem to exist (see Table 1). However, it is impossible to decide with certainty (due to various stellar and binary physics uncertainties) which predicted fate is the correct one (if any).

If very massive stars at LMC metallicity and with moderate rotation expand during their post-MS evolution (expected for low overshooting), then we predict the following evolution sequence for Mk 34:

$$\text{RLOF}_A \rightarrow \text{BH}_A \rightarrow \text{RLOF}_B \rightarrow \text{TZ}_{A+B}/\text{BH}_B, \qquad (1)$$

where the indices "A" and "B" mark the more- and less-massive component of Mk 34 respectively, $\text{BH}_{A/B}$ denotes the BH formation from a given component, and TZ_{A+B} means the formation of a Thorne–Żytkow object from both binary components in the second RLOF. The first RLOF (initiated by star A) is always found to be stable (TTMT/NTMT), while the second RLOF (donor: star B) can be either stable or dynamically unstable (CE). Additionally, the binary system may not survive the first RLOF while both stars merge, forming a single star that will be either subject to PSN (no remnant) or

---

[9] This range corresponds to the changing mass of the donor and accretor during RLOF.

will form a single BH:

$$RLOF_A \rightarrow single\ star \rightarrow PSN/BH. \qquad (2)$$

If such massive stars do not expand (for example, because of significant overshooting) the future evolutionary history proceeds without any binary interaction:

$$BH_A/PPSN_A/PSN_A \rightarrow BH_B/PPSN_B/PSN_B. \qquad (3)$$

Under very optimistic conditions (development and survival of CE initiated by a massive star with a radiative envelope and with a comparable-mass companion) Mk 34 may form a heavy BH–BH merger that would be a source of gravitational waves. Depending on our assumptions on mass loss and mixing in stellar interiors we find the formation of a $\sim 20 + 20\ M_\odot$ close BH–BH system that resembles the LIGO/Virgo detection of GW190408_181802 ($24.6^{+5.1}_{-3.4} + 18.4^{+3.3}_{-3.6}\ M_\odot$: Abbott et al. 2021) or a $\sim 30 + 30\ M_\odot$ BH–BH system that would look similar to GW150914 ($35.6^{+4.8}_{-3.0} + 30.6^{+3.0}_{-4.4}\ M_\odot$: Abbott et al. 2016) or to GW190828_063405 ($32.1^{+5.8}_{-4.0} + 26.2^{+4.6}_{-4.8}\ M_\odot$: Abbott et al. 2021). If this does not work, the formation of such LIGO/Virgo BH–BH mergers can still be obtained with more realistic CE input physics in the isolated binary evolution (Belczynski et al. 2016; Spera et al. 2019; Patton et al. 2021).

The detailed evolutionary estimates of a very massive star envelope-binding energy do not allow for a CE survival of the Mk 34 descendant binary even under very conservative assumptions (100% orbital energy used to eject the envelope with the help of internal energy of the gas and accretion luminosity from the inspiraling BH). If this is taken into account, then instead of forming a close BH–BH binary in the CE scenario, we encounter the formation of a Thorne–Żytkow object (BH sinks into the center of the post-MS massive star). This single object would first appear as a post-MS massive star (most likely a classical Wolf-Rayet star), that starts to expand, cooling off and getting redder as the envelope puffs up in response to the BH inspiraling in a H-rich envelope. Once the BH sinks into the star's core (the majority of star mass at this point) the accretion of helium is extremely rapid ($\gtrsim 1\ M_\odot\ min^{-1}$, as in a collapsar engine; Fryer & Woosley 1998) and the core disappears, and then the rest of the star is accreted as well and the object disappears entirely from the sky. Such a transient should be visible in optical/infrared (initial expansion of the envelope before it collapses onto the BH), although at this moment there are no available calculations of the light curve or spectra for such heavy mergers ($\sim 100\ M_\odot$ post-MS star and $\sim 20–30\ M_\odot$ BH). Observationally, various red novae/transients were proposed to be the outcome of CE mergers (Tylenda et al. 2005; Ivanova et al. 2013a; Kamiński et al. 2015; MacLeod et al. 2017b). It may be even possible that such a merger would lead to a gamma-ray burst (GRB). If there is enough angular momentum in the He core and BH, then such a configuration may lead to the formation of jets powering a GRB (Zhang & Fryer 2001). The angular-momentum transport in stellar interiors of massive stars is not fully constrained, although the low effective spins of LIGO/Virgo BH–BH mergers seem to indicate efficient angular-momentum transport in massive stars (Spruit 2002; Fuller et al. 2019; Bavera et al. 2020; Belczynski et al. 2020a). In such a case, a slowly spinning He-core–BH system would have only a small chance of producing a GRB. Another obstacle in producing a GRB in this case is $\sim 30\ M_\odot$ of H-rich envelope for jets to punch through. Yet, there are signs that

such jets do form in massive stars in CE mergers and they try to break out from stellar interiors (Thöne et al. 2015).

Another possibility for the future evolution of Mk 34 is to avoid the CE phase entirely, even if both stars in this binary expand. Because the orbital separation is not very large for this system, any RLOF encountered in the evolution is bound to happen when the donor star is not too large (a radiative envelope). Additionally, as the stars in Mk 34 are of similar mass, any RLOF is not bound to happen at an extreme mass ratio. Taking this into account, this binary may evolve through two episodes of stable RLOF (first initiated by initially more massive star, and then by the other star). Although such RLOF episodes may decrease the orbital separation, such orbit shrinking will be not large enough to lead to the formation of a close BH–BH binary (i.e., with a merger time smaller than the Hubble time) for the initial binary configuration of Mk 34. Instead, a wide BH–BH binary forms with separation as large as $\gtrsim 1000\ R_\odot$. Such a descendant of Mk 34 cannot be a LIGO/Virgo source, but could possibly be detected by microlensing observations. The magnification of the source in such a microlensing event would last months and would include bumps typical of a binary lens and would be potentially detectable in LMC.

Finally, it is also possible that neither of the stars in Mk 34 will experience any significant expansion in their post-MS evolution. In such a case, Mk 34 expands due to wind mass loss from both stars and forms a wide system when both components end their nuclear evolution (separation of $\sim 1000\ R_\odot$). Depending on the highly uncertain mixing physics and not fully constrained nuclear reaction rates (overshooting, rotation, convection, carbon fusion) that set the temperature/density in stellar cores, massive components of Mk 34 may or may not be a subject to significant mass loss associated with PPSN during oxygen burning. We predict the formation of a wide BH–BH system with comparable-mass BHs in the mass range $\sim 40–90\ M_\odot$. Alternatively, both stars in Mk 34 may be subject to a full-fledged pair instability and get disrupted in luminous PSNe (Higgins et al. 2021).

To summarize, we conclude that we cannot yet predict the fate of a massive binary such as Mk 34. The involved stellar and binary physics uncertainties are still too overwhelming. However, our study offers several conditional statements that shed light on the future evolution of this massive binary. If the stars in Mk 34 expand in their post-MS evolution, then they are bound to initiate two RLOF interactions (one by each component). Although the first interaction is always stable and does not threaten the survival of this system, the second one is more problematic. It is not at all clear if the second interaction will be dynamically stable. If it is not, then a CE phase develops and the most likely fate of the system is then the merger of the two binary components, possibly associated with a red nova or a GRB. If the second interaction is stable, then the RLOF will lead to the formation of a wide and massive BH–BH system with a merger time much larger than the Hubble time. Such a system is not a potential LIGO/Virgo source of high-frequency gravitational waves, but it may produce a microlensing event. If the stars in Mk 34 do not expand, which is also allowed by the current detailed evolutionary models, then we predict either the formation of a wide and potentially very massive BH–BH system, or the spectacular death of both stars in luminous PSNe that leave no BHs behind.

5. Conclusion

For the isolated binary BH–BH origin scenario, (i) there are a large number of input physics uncertainties or even unknowns (model parameters), (ii) the implementations of the physical processes that involve these uncertainties in the numerical codes are far from being based on first-principle physics, so even probing the full range of a given parameter might not get the right answer, and (iii) there are more parameters and thus uncertainties than commonly realized (there are at least $\sim$30 parameters in the isolated binary evolution channel, even though it is usually thought that only a small subset of them are really important in determining binary outcomes). Thus, strong conclusions that involve isolated binary evolution are unjustified at this time. In particular, reported branching ratios between various formation channels *all* involve isolated binary evolution models and these ratios need to be treated with caution.

As an example of how biases could enter the model comparisons, suppose that we use the rapid supernova engine model of Fryer et al. (2012), which naturally produces a $\sim$2–5 $M_\odot$ mass gap between neutron stars and BHs. Then, the discovery of the 2.6 $M_\odot$ object in GW190814 would rule strongly against isolated binary evolution and in favor of another channel, such as primordial BHs or multiple-generation mergers in dense stellar systems (e.g., two neutron stars could merge to make a $\sim$2.6 $M_\odot$ BH). But perhaps the delayed supernova engine model of Fryer et al. (2012) is a better description; in this model the compact objects with mass 2.6 $M_\odot$ are produced naturally and the isolated binary formation channel is perfectly viable. Or perhaps some other supernova model is selected by Nature, which would change the Bayes factor between the models that are considered. Similar considerations apply to the high-mass merger GW190521, which is consistent with binary stellar evolution given the substantial uncertainties (Belczynski 2020; Farmer et al. 2020; Kinugawa et al. 2021; Costa et al. 2021; Mehta et al. 2022; Vink et al. 2021).

We have focused on the specific system Mk 34, but our caveat extends to analyses of the full population of BH–BH mergers formed in isolated binary evolution. For example, Olejak et al. (2021) explored the effects on the BH–BH population that stem from different treatments of the common envelopes. Over the range of models they studied, the population characteristics varied drastically. For example, the BH–BH merger rate varied from 18 Gpc^{-3} yr^{-1} (consistent with the current LVC estimate of 15.3–38.8 Gpc^{-3} yr^{-1}: The LIGO Scientific Collaboration et al 2021) to 88 Gpc^{-3} yr^{-1}. The BH mass distribution can be consistent with the LVC estimate ($\propto M^{-1.5}$ below $\sim$40–50 $M_\odot$ and $\propto M^{-5.3}$ at higher masses), or very inconsistent with the estimate ($\propto M^{+2.7}$ for $M < 15\,M_\odot$ and $\propto M^{-3.3}$ for heavier BHs). The mass ratio distribution can have one peak or two peaks. To reiterate, even this broad range of predicted population characteristics does not include many other possible variations of aspects of stellar and binary evolution.

Moreover, while here we have solely focused on processes related to stellar and binary evolution (and their caveats), another layer of uncertainty in modeling the population of gravitational-wave sources arises from assumptions about the metallicity-specific cosmic star formation history (Chruslinska et al. 2019; Neijssel et al. 2019; Tang et al. 2020; Santoliquido et al. 2021). This is especially the case for the low-metallicity

Table 4
Maximum Radius and Stellar Mass, Core Mass, and Envelope Mass at TAMS from Different Combinations of Overshoot Fractions and Dutch Winds Scale Factors for the 144 $M_\odot$ ZAMS Star and the 131 $M_\odot$ ZAMS Star

Model	R_{Max} ($R_\odot$)	M_{TAMS} ($M_\odot$)	$M_{\mathrm{core,TAMS}}$ ($M_\odot$)	$M_{\mathrm{env,TAMS}}$ ($M_\odot$)
144 $M_\odot$ ZAMS Star				
δ_{ov} 0.12				
f_{wind} 1	>1967.640	94.018	66.578	27.440
f_{wind} 1.5	39.694	56.672	55.423	1.249
f_{wind} 2	25.870	30.662	28.014	2.648
δ_{ov} 0.16				
f_{wind} 1	>2000	93.139	68.443	24.696
f_{wind} 1.5	34.663	47.202	45.412	1.790
f_{wind} 2	24.192	27.978	25.227	2.750
δ_{ov} 0.2				
f_{wind} 1	>1129.641	91.070	70.021	21.049
f_{wind} 1.5	31.430	41.892	39.779	2.113
f_{wind} 2	23.346	26.517	23.794	2.723
δ_{ov} 0.33				
f_{wind} 1	46.046	62.221	60.782	1.438
f_{wind} 1.5	26.474	34.516	32.304	2.212
f_{wind} 2	21.062	23.249	20.738	2.511
δ_{ov} 0.4				
f_{wind} 1	36.335	53.797	52.095	1.702
f_{wind} 1.5	24.508	32.205	30.090	2.115
f_{wind} 2	20.183	22.135	19.744	2.391
δ_{ov} 0.5				
f_{wind} 1	30.383	48.080	46.399	1.682
f_{wind} 1.5	22.559	29.984	28.017	1.968
f_{wind} 2	19.189	20.896	18.737	2.159
131 $M_\odot$ ZAMS Star				
δ_{ov} 0.12				
f_{wind} 1	>2000	86.568	58.490	28.078
f_{wind} 1.5	40.419	62.672	52.644	10.028
f_{wind} 2	25.070	32.530	30.080	2.451
δ_{ov} 0.16				
f_{wind} 1	>2000	85.196	60.295	24.900
f_{wind} 1.5	33.693	49.404	47.764	1.640
f_{wind} 2	23.654	29.393	26.787	2.606
δ_{ov} 0.2				
f_{wind} 1	>2000	84.293	61.686	22.607
f_{wind} 1.5	29.989	42.995	40.967	2.029
f_{wind} 2	22.569	27.366	24.724	2.642
δ_{ov} 0.33				
f_{wind} 1	41.232	59.079	57.538	1.541
f_{wind} 1.5	24.696	34.222	31.988	2.234
f_{wind} 2	20.022	23.455	20.948	2.507
δ_{ov} 0.4				
f_{wind} 1	33.053	51.420	49.583	1.838
f_{wind} 1.5	23.301	32.049	29.895	2.154
f_{wind} 2	19.042	22.120	19.747	2.373
δ_{ov} 0.5				
f_{wind} 1	27.484	45.711	43.895	1.816
f_{wind} 1.5	21.311	29.517	27.527	1.990

Table 4
(Continued)

Model	R_{Max} $(R_\odot)$	M_{TAMS} $(M_\odot)$	$M_{\mathrm{core,TAMS}}$ $(M_\odot)$	$M_{\mathrm{env,TAMS}}$ $(M_\odot)$
f_{wind} 2	17.986	20.735	18.555	2.181

or high-redshift regime of star formation, which could yield a significant contribution to the observable population of BH–BH mergers (Dominik et al. 2013; Chruslinska & Nelemans 2019; Boco et al. 2021).

What must be done to reach a stage in which we can draw firm conclusions about the origins of BH–BH systems? More and better data may or may not help. For example, if multiple events point to compact objects in the ~ 2–$5\,M_\odot$ range, then this tells us that the lower mass gap is not a major feature of the mass distribution, but then the origin of such compact objects can be explained by multiple formation channels (isolated binaries, dynamics, or primordial BHs). On the other hand, some properties of individual events can point to particular origins. For example, an event with many cycles that is clearly highly eccentric would favor a dynamical origin, and a compact object with a mass $< 0.5\,M_\odot$ would signify a primordial BH. If LIGO/Virgo BH–BH mergers form with significant contribution from the isolated binary evolution channel, then our analysis applies and highlights the current inability to draw conclusions on branching ratios. In this case we emphasize that detailed work on the physics of stellar and binary evolution of massive stars is essential. Our work is not relevant to the case of LIGO/Virgo BH–BH mergers originating from other channels. However, similar uncertainty studies should be performed for other formation channels. Statistical analyses must be grounded in thorough and accurate physics and astrophysics regardless of the BH–BH formation channel.

Appendix
Winds-overshooting Grid

In Table 4 we presnt a grid of 131 $M_\odot$ and 144 $M_\odot$ models with several variations in overshooting and stellar winds.

ORCID iDs

A. Olejak https://orcid.org/0000-0002-6105-6492
S. Stevenson https://orcid.org/0000-0002-6100-537X
M. Coleman Miller https://orcid.org/0000-0002-2666-728X
J.-P. Lasota https://orcid.org/0000-0002-6171-8396
Paul A. Crowther https://orcid.org/0000-0001-6000-6920

References

Abbott, B. P., Abbott, R., Abbott, T. D., et al. 2016, PhRvL, 116, 061102
Abbott, R., Abbott, T. D., Abraham, S., et al. 2020a, PhRvL, 125, 101102
Abbott, R., Abbott, T. D., Abraham, S., et al. 2020b, ApJL, 896, L44
Abbott, R., Abbott, T. D., Abraham, S., et al. 2021, PhRvX, 11, 021053
Bavera, S. S., Fragos, T., Qin, Y., et al. 2020, A&A, 635, A97
Belczynski, K. 2020, ApJL, 905, L15
Belczynski, K., Bulik, T., Fryer, C. L., et al. 2010a, ApJ, 714, 1217
Belczynski, K., Dominik, M., Bulik, T., et al. 2010b, ApJL, 715, L138
Belczynski, K., Hirschi, R., Kaiser, E. A., et al. 2020b, ApJ, 890, 113
Belczynski, K., Holz, D. E., Bulik, T., & O'Shaughnessy, R. 2016, Natur, 534, 512
Belczynski, K., Kalogera, V., & Bulik, T. 2002, ApJ, 572, 407
Belczynski, K., Kalogera, V., Rasio, F. A., et al. 2008, ApJS, 174, 223
Belczynski, K., Klencki, J., Fields, C. E., et al. 2020a, A&A, 636, A104
Belczynski, K., Taam, R. E., Kalogera, V., Rasio, F. A., & Bulik, T. 2007, ApJ, 662, 504
Belczynski, K., Wiktorowicz, G., Fryer, C. L., Holz, D. E., & Kalogera, V. 2012, ApJ, 757, 91
Bestenlehner, J. M. 2020, MNRAS, 493, 3938
Bestenlehner, J. M., Gräfener, G., Vink, J. S., et al. 2014, A&A, 570, A38
Boco, L., Lapi, A., Chruslinska, M., et al. 2021, ApJ, 907, 110
Böhm-Vitense, E. 1958, ZAp, 46, 108
Bonanos, A. Z., Stanek, K. Z., Udalski, A., et al. 2004, ApJL, 611, L33
Brott, I., de Mink, S. E., Cantiello, M., et al. 2011, A&A, 530, A115
Castro, N., Fossati, L., Langer, N., et al. 2014, A&A, 570, L13
Chattopadhyay, D., Stevenson, S., Hurley, J. R., Bailes, M., & Broekgaarden, F. 2021, MNRAS, 504, 3682
Choi, J., Dotter, A., Conroy, C., et al. 2016, ApJ, 823, 102
Chruslinska, M., & Nelemans, G. 2019, MNRAS, 488, 5300
Chruslinska, M., Nelemans, G., & Belczynski, K. 2019, MNRAS, 482, 5012
Claret, A., & Torres, G. 2018, ApJ, 859, 100
Conti, P. S. 1975, MSRSL, 9, 193
Costa, G., Bressan, A., Mapelli, M., et al. 2021, MNRAS, 501, 4514
de Jager, C., Nieuwenhuijzen, H., & van der Hucht, K. A. 1988, A&AS, 72, 259
Dominik, M., Belczynski, K., Fryer, C., et al. 2012, ApJ, 759, 52
Dominik, M., Belczynski, K., Fryer, C., et al. 2013, ApJ, 779, 72
Farmer, R., Renzo, M., de Mink, S., Fishbach, M., & Justham, S. 2020, ApJL, 902, L36
Farr, B., Holz, D. E., & Farr, W. M. 2018, ApJL, 854, L9
Farr, W. M., Stevenson, S., Miller, M. C., et al. 2017, Natur, 548, 426
Farrell, E., Groh, J. H., Hirschi, R., et al. 2021, MNRAS, 502, L40
Fishbach, M., & Holz, D. E. 2020, ApJL, 904, L26
Franciolini, G., Baibhav, V., De Luca, V., et al. 2021, arXiv:2105.03349
Fryer, C. L., Belczynski, K., Wiktorowicz, G., et al. 2012, ApJ, 749, 91
Fryer, C. L., & Woosley, S. E. 1998, ApJL, 502, L9
Fuller, J., & Ma, L. 2019, ApJL, 881, L1
Fuller, J., Piro, A. L., & Jermyn, A. S. 2019, MNRAS, 485, 3661
Ge, H., Webbink, R. F., Chen, X., & Han, Z. 2015, ApJ, 812, 40
Gilkis, A., Shenar, T., Ramachandran, V., et al. 2021, MNRAS, 503, 1884
Glebbeek, E., Gaburov, E., Portegies Zwart, S., & Pols, O. R. 2013, MNRAS, 434, 3497
Gräfener, G., & Hamann, W. R. 2008, A&A, 482, 945
Grevesse, N., Noels, A., & Sauval, A. J. 1996, in ASP Conf. Ser., 99, Cosmic Abundances, ed. S. S. Holt & G. Sonneborn (San Francisco, CA: ASP), 117
Heger, A., Langer, N., & Woosley, S. E. 2000, ApJ, 528, 368
Higgins, E. R., Sander, A. A. C., Vink, J. S., & Hirschi, R. 2021, MNRAS, 505, 4874
Humphreys, R. M., & Davidson, K. 1979, ApJ, 232, 409
Humphreys, R. M., & Davidson, K. 1994, PASP, 106, 1025
Hurley, J. R., Pols, O. R., & Tout, C. A. 2000, MNRAS, 315, 543
Hurley, J. R., Tout, C. A., & Pols, O. R. 2002, MNRAS, 329, 897
Ivanova, N., Justham, S., Avendano Nandez, J. L., & Lombardi, J. C. 2013a, Sci, 339, 433
Ivanova, N., Justham, S., Chen, X., et al. 2013b, A&ARv, 21, 59
Kalogera, V., & Webbink, R. F. 1996, ApJ, 458, 301
Kamiński, T., Mason, E., Tylenda, R., & Schmidt, M. R. 2015, A&A, 580, A34
King, A. R., Davies, M. B., Ward, M. J., Fabbiano, G., & Elvis, M. 2001, ApJL, 552, L109
Kinugawa, T., Nakamura, T., & Nakano, H. 2021, MNRAS, 501, L49

Klencki, J., Nelemans, G., Istrate, A. G., & Chruslinska, M. 2021, A&A, 645, A54

Klencki, J., Nelemans, G., Istrate, A. G., & Pols, O. 2020, A&A, 638, A55

Köhler, K., Langer, N., de Koter, A., et al. 2015, A&A, 573, A71

Langer, N. 2012, ARA&A, 50, 107

Leung, S.-C., Nomoto, K., & Blinnikov, S. 2019, ApJ, 887, 72

Limongi, M., & Chieffi, A. 2018, ApJS, 237, 13

Lohr, M. E., Clark, J. S., Najarro, F., et al. 2018, A&A, 617, A66

Lombardi, J. C., Warren, J. S., Rasio, F. A., Sills, A., & Warren, A. R. 2002, ApJ, 568, 939

Lombardi, J. C. J., Proulx, Z. F., Dooley, K. L., et al. 2006, ApJ, 640, 441

MacLeod, M., Antoni, A., Murguia-Berthier, A., Macias, P., & Ramirez-Ruiz, E. 2017a, ApJ, 838, 56

MacLeod, M., & Loeb, A. 2020, ApJ, 893, 106

MacLeod, M., Macias, P., Ramirez-Ruiz, E., et al. 2017b, ApJ, 835, 282

MacLeod, M., Ostriker, E. C., & Stone, J. M. 2018, ApJ, 863, 5

Mahy, L., Sana, H., Abdul-Masih, M., et al. 2020, A&A, 634, A118

Mandel, I., & Broekgaarden, F. S. 2021, arXiv:2107.14239

Marchant, P., Pappas, K. M. W., Gallegos-Garcia, M., et al. 2021, A&A, 650, A107

Marchant, P., Renzo, M., Farmer, R., et al. 2019, ApJ, 882, 36

Massey, P., Penny, L. R., & Vukovich, J. 2002, ApJ, 565, 982

Mehta, A. K., Buonanno, A., Gair, J., et al. 2022, ApJ, 924, 39

Mennekens, N., & Vanbeveren, D. 2014, A&A, 564, A134

Miller-Jones, J. C. A., Bahramian, A., Orosz, J. A., et al. 2021, Sci, 371, 1046

Mondal, S., Belczyński, K., Wiktorowicz, G., Lasota, J.-P., & King, A. R. 2020, MNRAS, 491, 2747

Neijssel, C. J., Vigna-Gómez, A., Stevenson, S., et al. 2019, MNRAS, 490, 3740

Neijssel, C. J., Vinciguerra, S., Vigna-Gómez, A., et al. 2021, ApJ, 908, 118

Nitz, A. H., & Capano, C. D. 2021, ApJL, 907, L9

Nugis, T., & Lamers, H. J. G. L. M. 2000, A&A, 360, 227

Olejak, A., Belczynski, K., Bulik, T., & Sobolewska, M. 2020, A&A, 638, A94

Olejak, A., Belczynski, K., & Ivanova, N. 2021, A&A, 651, A100

Ossowski, M. 2021, A&A, 649, A57

Patton, R. A., Sukhbold, T., & Eldridge, J. J. 2021, arXiv:2106.05978

Pavlovskii, K., & Ivanova, N. 2015, MNRAS, 449, 4415

Pavlovskii, K., Ivanova, N., Belczynski, K., & Van, K. X. 2017, MNRAS, 465, 2092

Paxton, B., Bildsten, L., Dotter, A., et al. 2011, ApJS, 192, 3

Paxton, B., Cantiello, M., Arras, P., et al. 2013, ApJS, 208, 4

Paxton, B., Marchant, P., Schwab, J., et al. 2015, ApJS, 220, 15

Paxton, B., Schwab, J., Bauer, E. B., et al. 2018, ApJS, 234, 34

Paxton, B., Smolec, R., Schwab, J., et al. 2019, ApJS, 243, 10

Peters, P. C. 1964, PhRv, 136, 1224

Podsiadlowski, P., Joss, P. C., & Hsu, J. J. L. 1992, ApJ, 391, 246

Pollock, A. M. T., Crowther, P. A., Tehrani, K., Broos, P. S., & Townsley, L. K. 2018, MNRAS, 474, 3228

Pols, O. R., Schröder, K.-P., Hurley, J. R., Tout, C. A., & Eggleton, P. P. 1998, MNRAS, 298, 525

Qin, Y., Fragos, T., Meynet, G., et al. 2018, A&A, 616, A28

Rolleston, W. R. J., Trundle, C., & Dufton, P. L. 2002, A&A, 396, 53

Sana, H., de Mink, S. E., de Koter, A., et al. 2012, Sci, 337, 444

Santoliquido, F., Mapelli, M., Giacobbo, N., Bouffanais, Y., & Artale, M. C. 2021, MNRAS, 502, 4877

Schneider, F. R. N., Izzard, R. G., Langer, N., & de Mink, S. E. 2015, ApJ, 805, 20

Schnurr, O., Casoli, J., Chené, A. N., Moffat, A. F. J., & St-Louis, N. 2008, MNRAS, 389, L38

Schootemeijer, A., Langer, N., Grin, N. J., & Wang, C. 2019, A&A, 625, A132

Scott, L. J. A., Hirschi, R., Georgy, C., et al. 2021, MNRAS, 503, 4208

Shao, Y., & Li, X.-D. 2021, ApJ, 920, 81

Shenar, T., Sana, H., Marchant, P., et al. 2021, A&A, 650, A147

Smith, N. 2014, ARA&A, 52, 487

Spera, M., Mapelli, M., Giacobbo, N., et al. 2019, MNRAS, 485, 889

Spruit, H. C. 2002, A&A, 381, 923

Stevenson, S., Sampson, M., Powell, J., et al. 2019, ApJ, 882, 121

Stevenson, S., Vigna-Gómez, A., Mandel, I., et al. 2017, NatCo, 8, 14906

Tang, P. N., Eldridge, J. J., Stanway, E. R., & Bray, J. C. 2020, MNRAS, 493, L6

Tehrani, K. A., Crowther, P. A., Bestenlehner, J. M., et al. 2019, MNRAS, 484, 2692

The LIGO Scientific Collaboration, et al. 2021, ApJL, 913, L7

Thöne, C. C., de Ugarte Postigo, A., Fryer, C. L., & Kann, D. A. 2015, in IAU Symp. 313, Extragalactic Jets from Every Angle, ed. F. Massaro, C. C. Cheung, E. Lopez, & A. Siemiginowska (Cambridge: Cambridge Univ. Press), 396

Thorne, K. S., & Zytkow, A. N. 1977, ApJ, 212, 832

Tylenda, R., & Kamiński, T. 2016, A&A, 592, A134

Tylenda, R., Soker, N., & Szczerba, R. 2005, A&A, 441, 1099

van den Heuvel, E. P. J., Portegies Zwart, S. F., & de Mink, S. E. 2017, MNRAS, 471, 4256

Vanbeveren, D. 1991, A&A, 252, 159

Vanbeveren, D., De Loore, C., & Van Rensbergen, W. 1998, A&ARv, 9, 63

Vigna-Gómez, A., Neijssel, C. J., Stevenson, S., et al. 2018, MNRAS, 481, 4009

Vink, J. S., Brott, I., Gräfener, G., et al. 2010, A&A, 512, L7

Vink, J. S., de Koter, A., & Lamers, H. J. G. L. M. 2001, A&A, 369, 574

Vink, J. S., Higgins, E. R., Sander, A. A. C., & Sabhahit, G. N. 2021, MNRAS, 504, 146

Vink, J. S., Muijres, L. E., Anthonisse, B., et al. 2011, A&A, 531, A132

Vitale, S., Lynch, R., Sturani, R., & Graff, P. 2017, CQGra, 34, 03LT01

Webbink, R. F. 1984, ApJ, 277, 355

Wiktorowicz, G., Belczynski, K., & Maccarone, T. 2014, Binary Systems, their Evolution and Environments (Ulaanbaatar, Mongolia, September 1–5, 2014) 37

Woosley, S. E. 2017, ApJ, 836, 244

Xu, X.-J., & Li, X.-D. 2010, ApJ, 722, 1985

Yusof, N., Hirschi, R., Meynet, G., et al. 2013, MNRAS, 433, 1114

Zevin, M., Bavera, S. S., Berry, C. P. L., et al. 2021, ApJ, 910, 152

Zevin, M., Spera, M., Berry, C. P. L., & Kalogera, V. 2020, ApJL, 899, L1

Zhang, W., & Fryer, C. L. 2001, ApJ, 550, 357